Available online at www.sciencedirect.com
SCIENCE DIRECT®

Journal of the European Ceramic Society 24 (2004) 441–448

www.elsevier.com/locate/jeurceramsoc

Micro-thermal analysis for advanced silicon nitrides

Jiping Ye[a], Akira Okada[b,*]

[a]Nissan Arc Co. Ltd., Yokosuka, 237-0061, Japan
[b]Nissan Motor Co. Ltd., Yokosuka, 237-8523, Japan

Abstract

Microstructures of three grades of gas-pressure-sintered silicon nitride materials, SN-H, SN-L and SN-A, were evaluated with a scanning electron microscopy, an atomic force microscopy and a micro-thermal analyzer. Thermal images corresponding to local thermal conductance distribution were obtained with the micro-thermal analyzer, and the thermal conductivity was confirmed to be higher in silicon nitride grains and lower in grain boundaries. Thermal analyses at particular areas in the microstructures revealed that the local thermal conductivity of silicon nitride grains is higher in SN-L than in SN-H. This seems inconsistent with the bulk thermal conductivities because SN-H exhibited the highest thermal conductivity of 132.3 W/(m K), which is considerably greater than that of SN-L of 104.7 W/(m K). The discrepancy between the grain and bulk thermal conductivities is discussed.

Keywords: Atomic force microscopy; Microstructure-final; Microthermal analysis; Si_3N_4; Thermal conductivity

1. Introduction

Since silicon nitride potentially has a high thermal conductivity due to its strong chemical bonding and light constituting elements, considerable work has been done for enhancing the conductivity. It has been reported that promoting grain growth and selecting a suitable additive system for liquid phase sintering are effective for high thermal conductivity, and thermal conductivity higher than 120 W/(m K) has been achieved.[1–3] Further improvements have been achieved with texture control that allows the elongated silicon nitride grains to align in plane or uniaxial directions.[4–7] Such elongated grain structures exhibit high thermal conductivity along the elongated grain directions while the direction perpendicular to the elongated grains has low thermal conductivity. The high thermal conductivity of 162 W/(m K) was achieved with an aligned grain structure uniaxially along the particular direction, coupled with intensive grain growth.[7,8]

It has been pointed out that high thermal conductivity is difficult to be explained with the elongated microstructures because the mean free pass of phonon in silicon nitride is estimated to be around 20 nm at room temperature and this is considerably smaller than the grain dimension.[9] In addition, a simple calculation based on a composite model of silicon nitride grains and glassy phases concluded that thermal conductivity of silicon nitrides are insensitive to the grain size in the region approximately greater than 1 μm, assuming the thickness of grain boundary glass films to be 1 nm.[10] The internal defect structure rather than grain size was therefore thought to govern the thermal conductivity, and lattice oxygen was revealed to be responsible for the phonon scattering to reduce thermal conductivity.[11,12] However, silicon nitride grain has an anisotropy in thermal conductivity, and it was reported to be 180 W/(m K) along the *c*-axis and 69 W/(m K) along the a-axis.[13] Therefore, the elongated grain structure of silicon nitride with a high aspect ratio is expected to have higher thermal conductivity along the elongated grains than that with a low aspect ratio because the grains usually grow along the *c*-axis direction. For revealing the detailed mechanism of thermal conductance, it is important to evaluate local thermal conductivities.

Actually, the local thermal diffusivity has been evaluated with a photo-thermal method, and already applied to silicon nitride,[13,14] aluminum nitride[15] and ceramic matrix composites.[16] In recent years, a scanning thermal microscope has attracted considerable attention

* Corresponding author. Tel.: +81-468-67-5196; fax: +81-468-65-5796.
E-mail address: okada-a@mail.nissan.co.jp (A. Okada).

0955-2219/03/$ - see front matter © 2003 Elsevier Ltd. All rights reserved.
doi:10.1016/S0955-2219(03)00208-5

Table 1
Silicon nitride materials used in this work

Materials	Chemical composition of sintering aids	Sintering conditions			Density Mg/m^3	Thermal conductivity W/(m K)
		Temperature (K)	Time (h)	N_2 Pressure (MPa)		
SN-H	1 mol% Y_2O_3 and 1 mol% Nd_2O_3	2473	12	29.4	3.20	132.3
SN-L	0.5 mol% Y_2O_3, 0.5 mol% Nd_2O_3 and 1 mol% MgO	2273	8	29.4	3.22	104.7
SN-A	2 mol% Y_2O_3 and 2 mol% Al_2O_3	2173	8	0.88	3.23	~60

as an alternative technique since it is commercially available.[17–22] The scanning thermal microscope comes under the category of scanning probe microscopy, in which a miniaturized thermal probe is used not only to heat a local position but also to detect the temperature. We have applied this technique to silicon nitrides, and investigated local thermal response at grains and boundaries.[23,24] In the present paper, we discuss the thermal response obtained by this technique, in conjunction with images obtained by AFM and SEM.

2. Experimental procedure

Three grades of silicon nitride ceramics, SN-H, SN-L and SN-A, were used in the present study (see Table 1). The SN-H specimen was prepared from a powder mixture of β-Si_3N_4 containing 1 mol% Y_2O_3 and 1 mol% Nd_2O_3, and disk-shaped powder compacts were formed. The powder compacts were sintered at 2273 K for 4 h under 29.4 MPa nitrogen gas, and additional firing was performed at temperatures up to 2473 K for 12 h so as to enhance grain growth. SN-L was prepared from β-Si_3N_4 powder containing 0.5 mol% Y_2O_3, 0.5 mol% Nd_2O_3 and 1 mol% MgO as sintering aids. The powder compacts were sintered at 2173 K for 4 h under 0.88 MPa nitrogen gas and the additional firing to coarsen the grains was performed at 2273 K for 8 h under 29.4 MPa nitrogen gas. Note that ultimate sintering temperature for SN-H is higher than SN-L, and coarsen microstructure is expected for SN-H. The SN-A was prepared from β-Si_3N_4 powder mixed with 2 mol% Al_2O_3 and 2 mol% Y_2O_3. The powder compacts were sintered at 2173 K for 8 h under 0.88 MPa nitrogen gas. The materials were fully dense since the density of SN-H, SN-L and SN-A was 3.20, 3.22 and 3.23 Mg/m^3, respectively. According to laser flash measurements, the thermal conductivity of SN-H was 132.3 W/(m K), and this was considerably higher than the 104.7 W/(m K) determined for SN-L. The thermal conductivity of SN-A is estimated to be around 60 W/(m K) from the similar lots of the material. The low thermal conductivity of SN-A is obviously due to the addition of Al to silicon nitride to form β′-SiAlON solid solution. Specimens for examining the texture were prepared by mechanical polishing, followed by plasma etching with CF_4 gas. The detailed procedure has been described elsewhere.[1–3,23,24]

A scanning electron microscope (SEM, S-4700, Hitachi, Japan) was used to observe the microstructure of Si_3N_4 materials. The plasma-etched specimens were sputter-coated with platinum to avoid charge up, prior to the SEM observation. An atomic force microscope (AFM, Nanoscope-IIIa/D3100M microscope, Digital Instruments Ltd., Santa Barbara, CA) was also used to observe the microstructure. Topographic images were obtained in a tapping mode using a Si strap cantilever, which has a spring constant of around 50 N/m and a resonance frequency of approximate 350 kHz.

A μTA microscope (μTA 2990, TA Instruments Inc., New Castle, DE) was used for micro-thermal analysis to obtain thermal images corresponding to the Si_3N_4 microstructure. This microscope is based on an AFM, in which the normal probe is replaced with a wire probe having a resistive heater at the tip. Fig. 1 shows

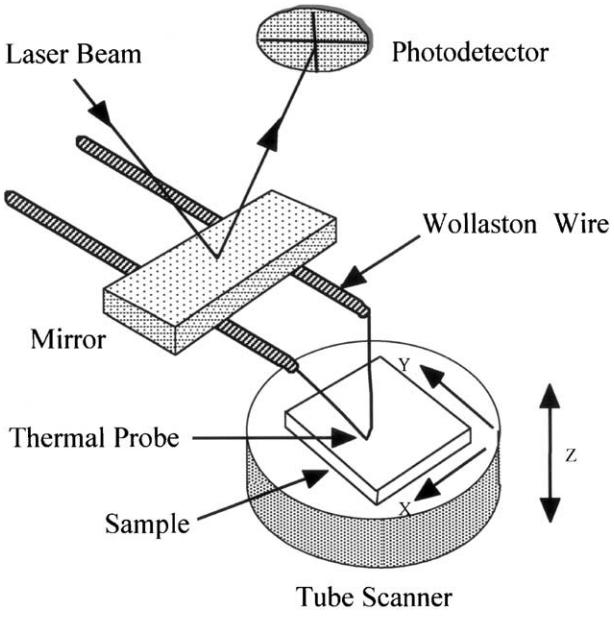

Fig. 1. A schematic diagram of a micro-thermal analyzer. The thermal sensor is a fine V-shaped platinum wire supported by Wollaston wires consisting of a silver sheath and a fine platinum core.

a schematic diagram of the thermal microscope. The thermal probe is a V-shaped fine platinum wire, supported by Wollaston wires. This tip acts as a localized heater when an electric current passes through the wire, and it also works as a thermal sensor by monitoring the electric resistance of the probe. In a scanning thermal microscopy mode, the wire tip is heated and kept at a constant temperature higher than the specimen, so that heat can flow from the tip through the specimen when the former comes in contact with the latter. The thermal images corresponding to the thermal conductance distribution were thus obtained by mapping the supply power to the measuring tip at a constant temperature.

Local thermal conductance was also evaluated. The probe was placed at a selected point on the surface and the temperature of the probe was ramped up to 673 K. The differential supply power for the tip of the probe between the conditions in contact with the specimen and placed in the air is calculated as the tip temperature rises.

3. Results and discussion

Fig. 2 shows the microstructures of SN-H observed with SEM, AFM and μTA. It is seen from the SEM micrographs that the material has a bimodal grain size distribution. The large grains have several tens of micrometers and small grains are of several micrometers. The small grains are rather concentrated in a particular area, and the area of the large grains is larger than the small-grained area. The sintering aids of rare earth elements, which are brightly seen in SEM micrographs due to the high emission rate of secondary electrons, are mainly found within the small-grained area as a multi-junction glass phase. Close-up of the small-grained areas revealed that the dimensions of small rod-shaped silicon nitrides are approximately 1 μm in diameter and several micrometers in length, and the intermediate dimensions between large and small grains are not so often found. Therefore, it is thought that large grains are produced as a result of rapid growth of the small

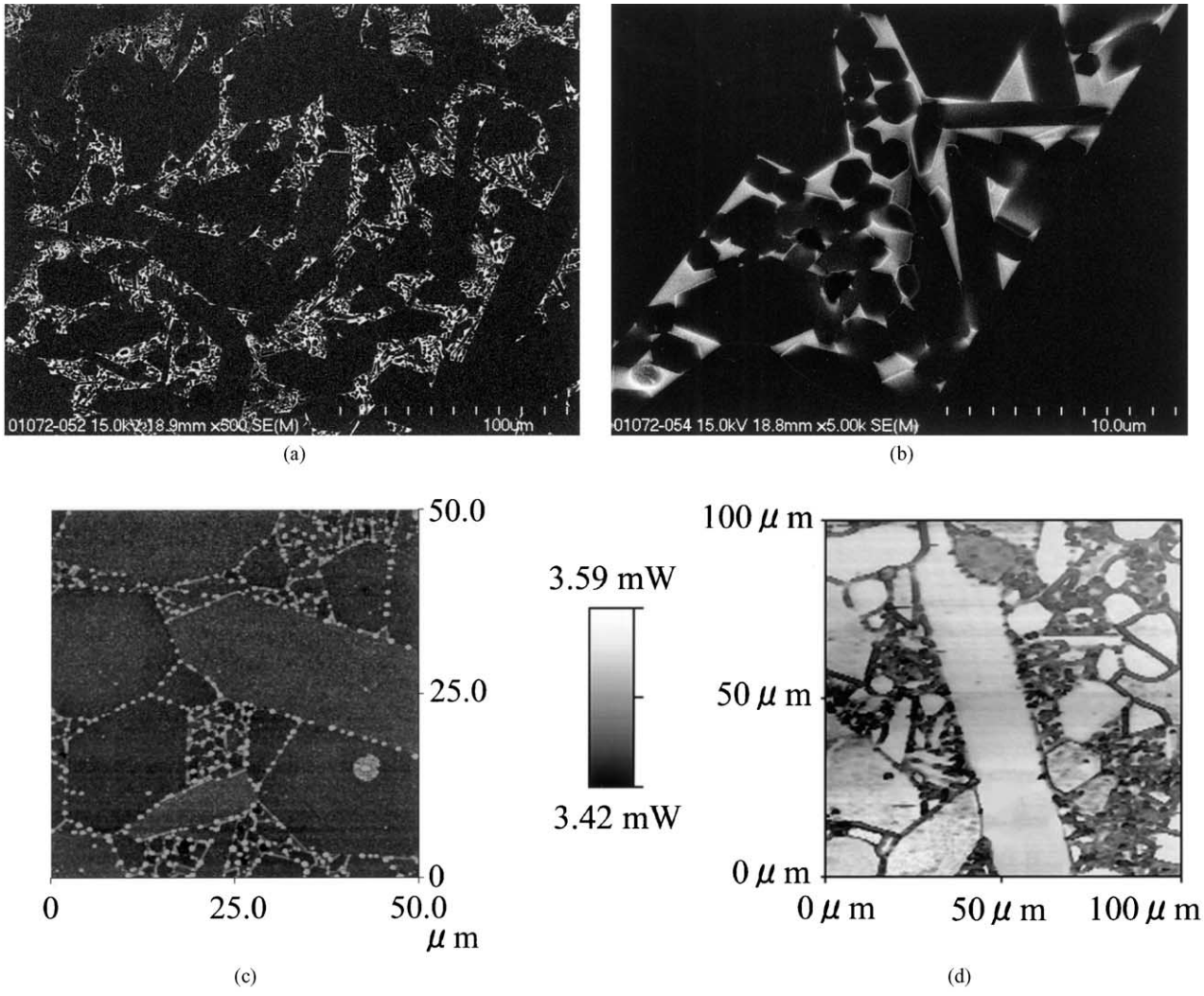

Fig. 2. Microstructure observations of silicon nitride: SN-H. (a) a scanning electron micrograph, (b) a close-up image of scanning electron microscopy for the area of the small grains (c) an AFM topographic image with a line analysis, and (d) a thermal image.

grains, and the liquid phase having been present in the original position of the large grains has been squeezed out to be concentrated in the small-grained area. Note that the small grains remain without experiencing intensive grain growth, and the glass phase is concentrated there as a result of squeezing out from the large grains developed. The large-grained microstructure found in SN-H is due to the prolonged soaking time of 16 h at 2473 K because the similar microstructure has been reported for silicon nitride produced in the same sintering condition.[7,8]

Since the contrast in scanning electron micrographs is governed by the difference in the secondary electron emission rates of the constituting elements, the glassy phase condensed in the small-grained area is clearly visualized. On the other hand, thin glass films between two neighboring grains are unclear due to slight difference in secondary electron emission rate from silicon nitride grains because the SiO_2 rich amorphous phase with low concentration of rare earth elements forms the glass films.[25] This also suggests that the condition of the plasma etching is too weak for SEM observation to visualize the grain boundaries clearly while the presence of the thin glass films between two grains was confirmed by AFM images. In the AFM observation, the grain boundaries were clearly seen. This indicates that the sensitivity of AFM to the height direction is much greater than SEM.

Grain boundaries were also visualized with μTA as areas of low thermal conductivity. It might be simply thought that the thin glass films are easily detected with μTA because the thermal conductivity of the glass phase is much lower than silicon nitride grains. The actual explanation is, however, not so simple since the glass films are very thin while having very low thermal conductivity. The thermal conductivity of the glass is

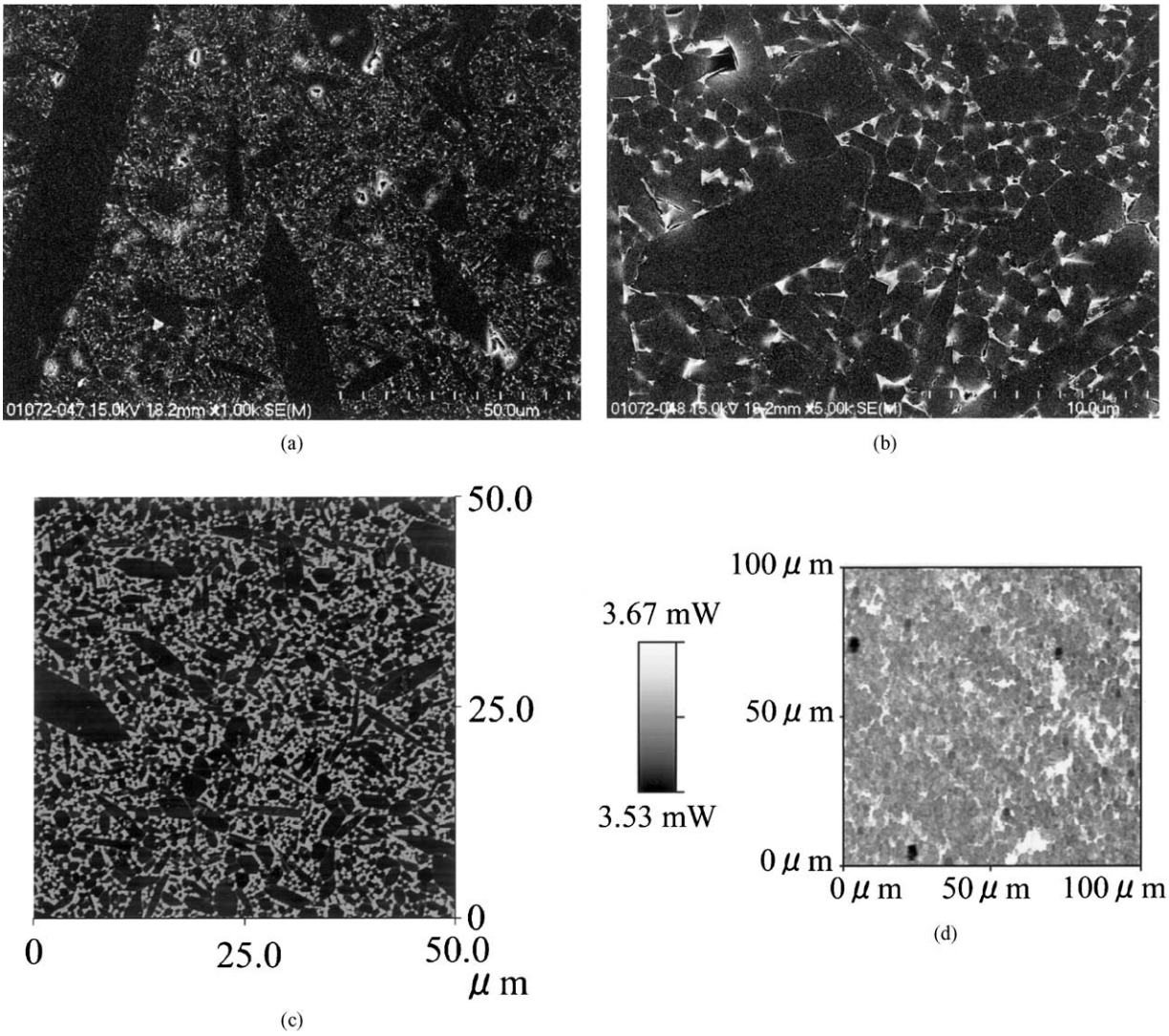

Fig. 3. Microstructure observations of silicon nitride: SN-L. (a) a scanning electron micrograph, (b) a close-up image of scanning electron microscopy for the fine matrix grains, (c) an AFM topographic image, (d) a thermal image.

around 1 W/(m K), and this is considerably lower than that of silicon nitride grains, which is estimated to be higher than 100 W/(m K). However, the film thickness is only 1 nm, and this is much smaller than the grain size of silicon nitride. Considering the ratios of thermal conductivity and thickness between grain and boundary phase, the thermal resistance of the glass film may be not important for total thermal conductance. From the thermal images obtained, the grain boundary looks broader than true thickness and seems to have higher thermal conductivity than the true value. Thin glass film boundaries seem to interfere with the heat flow and to broaden the apparent boundary thickness of low thermal conductance. This is because the heat flow is obstructed by the presence of the grain boundary wall of low thermal conductivity when the thermal tip is placed on the surface near the boundary. The broadening effect of grain boundaries is expected to be more significant when the interface boundary is slanted to the perpendicular direction of specimen. It should be noted that the similar μTA images are obtained for specimen without plasma etching because the μTA images correspond to the local thermal conductivity and are independent of the surface asperity. This is very different from the AFM and SEM techniques, in which the texture observation requires some techniques of visualizing grain structures.

Fig. 3 shows the microstructure images of SN-L obtained with SEM, AFM and μTA. The SEM micrographs reveal that the material has a bimodal grain size distribution, and the small-grained area is considerably greater than the large-grained one. The dimension of the large grains is approximately several tens of micrometers and most of the small grains are 1–2 μm. Such

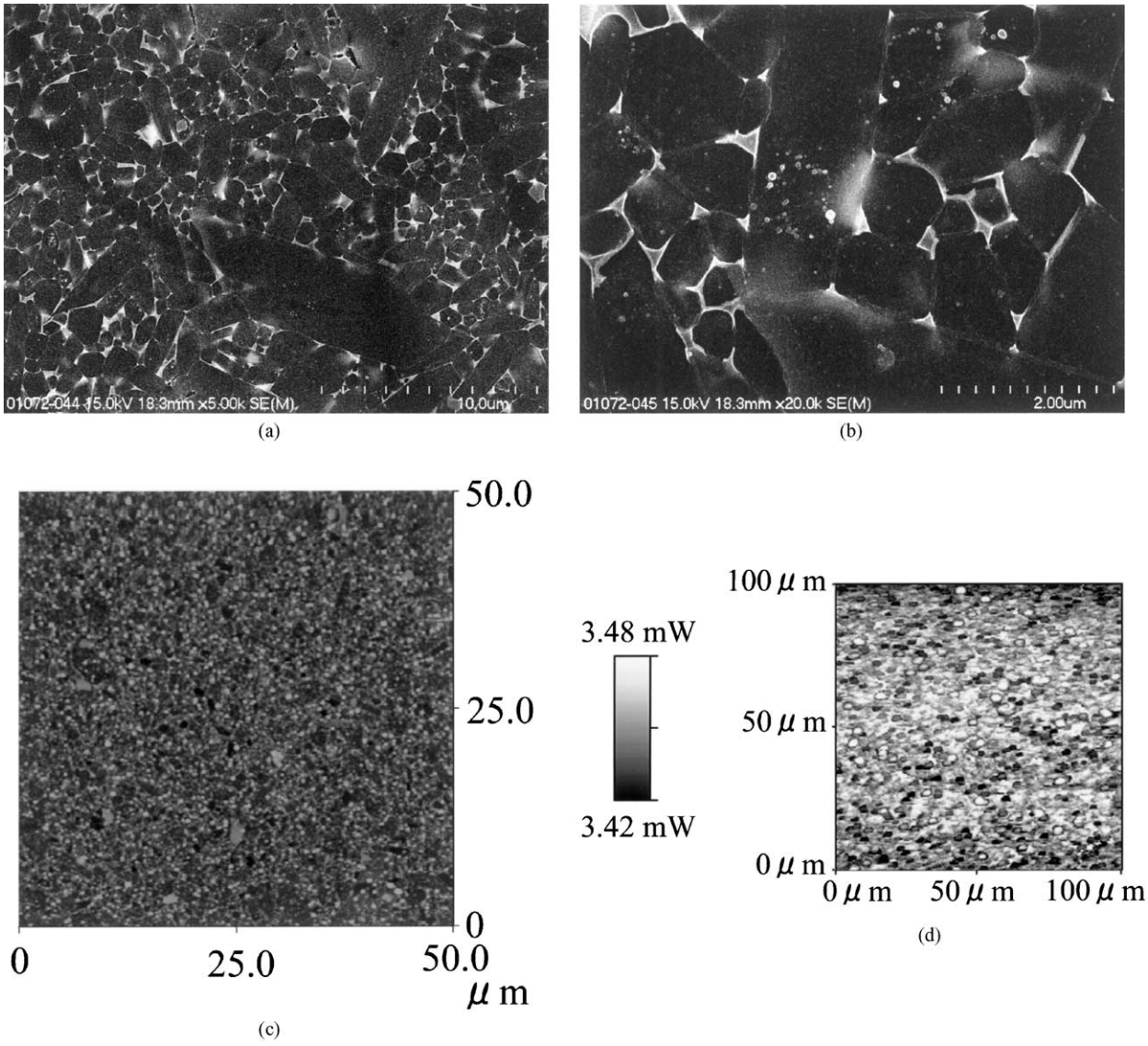

Fig. 4. Microstructure observations of silicon nitride: SN-A. (a) a scanning electron micrograph, (b) a close-up image of scanning electron microscopy, (c) an AFM topographic image, (d) a thermal image.

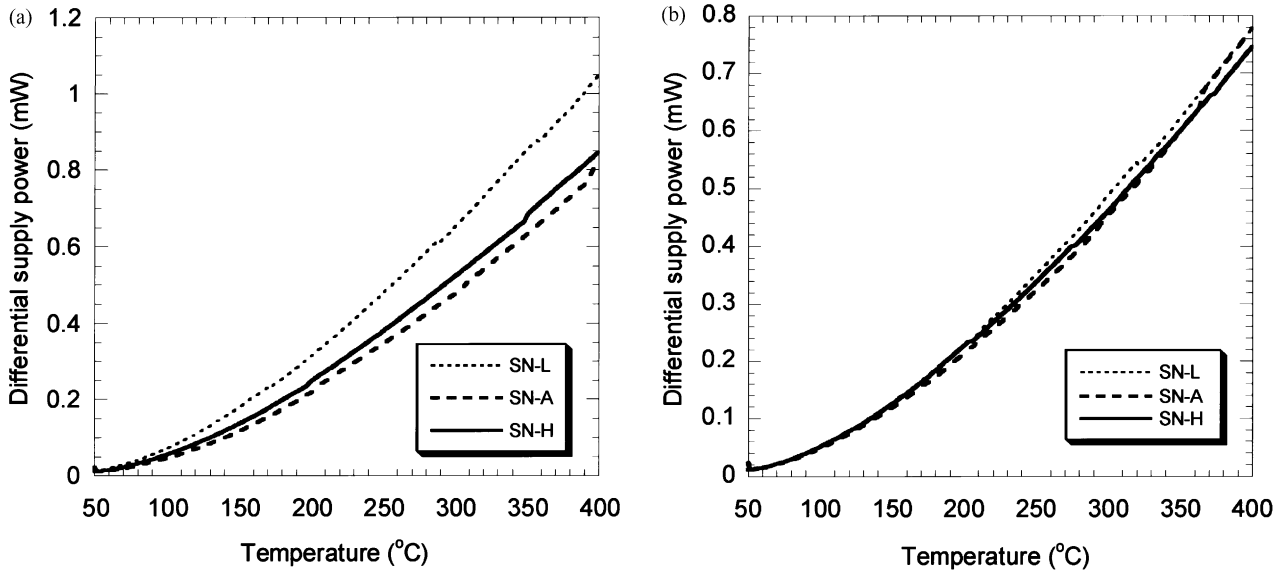

Fig. 5. Localized thermal analyses of silicon nitrides: SN-H, SN-L and SN-A. (a) Si_3N_4 grains and (b) grain boundaries.

microstructure is basically controlled with the sintering temperature and soaking time because silicon nitride produced in the condition of the same sintering temperature exhibited a similar microstructure.[1,2] The rare earth elements used for sintering aids form a glassy phase present at multi-junction grain boundaries. However, the fraction of the glassy phase in the small-grained area of SN-L is smaller than that of SN-H. This confirms that the glassy phase is squeezed out from large-grained area during the grain growth stage and consequently concentrates in the small-grained area. The AFM image shown in Fig. 3c is similar to the SEM image, and the similar bimodal structure is seen. The details in the small-grained structure are unclear in comparison with the SN-H image due to smaller microstructure. In general, the AFM is capable of providing accurate measurements in the height direction but the accuracy of measurements in horizontal directions is limited with the tip radius of the cantilever. The poor thermal image of SN-L is obviously due to the limited resolution in horizontal directions because the dimension of the small grains is comparable to the resolution of the thermal probe.

Fig. 4 shows the microstructures of SN-A obtained with SEM, AFM and μTA. From the SEM micrographs, the dimension of the major grain is found to be approximately 1–2 μm and the small amount of elongated grains of approximately 10 μm are seen. The AFM image also indicates the fine-grained microstructure while the detailed structure is invisible. The thermal image is unclear obviously due to the fine-grained microstructure comparable with the thermal probe resolution.

Comparing the images of SEM, AFM and μTA for three grades of silicon nitride materials, the SEM images are clearly seen even at high magnification. The SEM observes the difference in secondary electron emission rates between silicon nitride grain and the grain boundary glass phase containing rare earth elements. The horizontal resolution of scanning probe microscopy such as AFM and μTA is generally limited with the tip radius of microprobe, while in some cases the microstructure is visualized clearly. In the SN-H material, the thin film boundaries, which are hardly seen in SEM observation, are clearly observed in AFM and μTA.

Fig. 5 shows the results of local thermal analyses for SN-H, SN-L and SN-A. The differential supply power ΔP for grains and boundaries was plotted against the tip temperature of the probe. The position of grains was selected on a large grain found in the microstructure and the position of grain boundary was chosen at a glass phase present among large grains. The differential supply power increases with tip temperature in all the measurements. The increasing rates for the silicon nitride grains depend on the materials while those for grain boundaries are similar to each other. The differential power supply for SN-L is the greatest among three materials investigated. Compared to SN-L, the thermal conductivities of SN-H and SN-A are estimated to be lower. The low thermal conductivity of silicon nitride grain in SN-A is obviously due to the incorporation of Al ion into the grain as forming a solid solution of β′-SiAlON. The low thermal conductivity of the grain in SN-H is attributed to the extremely high sintering temperature, which enhances the solubility of foreign ions such as oxygen and rare earth elements used as sintering aids.[24]

The local thermal conductance of silicon nitride grains in SN-L is higher than SN-H, while the bulk thermal conductivity of SN-L is lower than SN-H. This discrepancy may be explained in terms of microstructure since the grain boundary glass film, which has

low thermal conductivity and constant thickness, degrades the bulk thermal conductivity. This effect is greater in SN-L than SN-H because the smaller grain size of SN-L leads to higher possibility of encountering the boundaries as heat flows. The high bulk thermal conductivity of SN-H, therefore, results from the large grains.

The thermal conductivity may be calculated from the thermal response obtained from scanning probe microscope, and this method was successfully applied to thin films [26,27]. However, this is not always possible for polycrystalline solids because the heat flow from the probe is influenced by the circumstance around the particular grains. In the case of thin films, the minimum thickness for determining the local thermal conductivity was established experimentally [26]. However, the requirements for polycrystalline solids have not yet established and further works are required.

4. Conclusions

Three grades of gas-pressure-sintered silicon nitride materials, SN-H, SN-L, and SN-A, were evaluated with a scanning electron microscopy, an atomic force microscopy and a micro-thermal analyzer. The micro-thermal analyzer revealed the local thermal conductance distribution of materials and confirmed that thermal conductivity is high in silicon nitride grains and low in grain boundaries. The local thermal analysis revealed that the thermal conductivity of silicon nitride grain in SN-L is higher than that of SN-H and SN-A. However, the bulk thermal conductivities for SN-H, SN-L, and SN-A were 132.3 W/(m K), 104.7 W/(m K), and around 60 W/(m K), respectively. The local thermal conductance of silicon nitride grains in SN-L is higher than SN-H, but the bulk thermal conductivity of SN-L is lower than SN-H. The explanation for this discrepancy was that the grain boundary glass phase of low thermal conductivity degrades the thermal conductivity and this effect is greater in SN-L because the smaller grain size of SN-L leads to a higher possibility of encountering the boundaries as heat flows. For a similar reason, the high bulk thermal conductivity of SN-H was thought to result from large grains. The low thermal conductance in silicon nitride grains in SN-H was thought to result from the high temperature heat treatment, and it was thought that the high temperature soaking degrades the thermal conductance of the silicon nitride grains by incorporating the impurity such as oxygen and rare earth elements employed for sintering aids.

Acknowledgements

We would like to thank Mr. N. Kojima for assisting with SEM work and Mr. T. Hori for assisting with material preparation. This work has been supported by The New Energy Development Organization (NEDO) as part of the Synergy Ceramics Project under the Industrial Science and Technology Frontier (ISFT) program promoted by the Agency of Industrial Science and Technology (AIST), Ministry of Economy, Trade and Industry (METI), Japan. One of the authors (Akira Okada) is a member of the Joint Research Consortium of Synergy Ceramics.

References

1. Hirosaki, N., Okamoto, Y., Ando, M., Munakata, F. and Akimune, Y., Effect of grain growth on the thermal conductivity of silicon nitride. *J. Ceram. Soc. Jpn.*, 1996, **104**, 49–53.
2. Hirosaki, N., Okamoto, Y., Ando, M., Munakata, F. and Akimune, Y., Thermal conductivity of gas-pressure-sintered silicon nitride. *J. Am. Ceram. Soc.*, 1996, **79**, 2878–2882.
3. Okamoto, Y., Hirosaki, N., Ando, M., Munakata, F. and Akimune, Y., Effect of sintering additive composition on the thermal conductivity of silicon nitride. *J. Mater. Res.*, 1998, **13**, 3473–3474.
4. Hirao, K., Watari, K., Brito, M. E., Toriyama, M., Kanzaki, S. and High thermal conductivity in silicon nitride with anisotropic microstructure, J., Am. *Ceram. Soc.*, 1996, **79**, 2485–2488.
5. Hirosaki, H., Ando, M., Okamoto, Y., Munakata, F., Akimune, Y., Hirao, K., Watari, K., Brito, M. E., Toriyama, M. and Kanzaki, S., Effect of alignment of large grains on the thermal conductivity of self-reinforced β-silicon nitride. *J. Ceram. Soc. Jpn.*, 1996, **104**, 1171–1173.
6. Okamoto, Y., Hirosaki, N., Ando, M., Munakata, F. and Akimune, Y., Thermal conductivity of self-reinforced silicon nitride containing large grains aligned by extrusion pressing. *J. Ceram. Soc. Jpn.*, 1997, **105**, 631–633.
7. Akimune, Y., Munakata, F., Matsuo, K., Hirosaki, N., Okamoto, Y. and Mizono, K., Raman spectroscopic analysis of structural defects in hot isostatically pressed silicon nitride. *J. Ceram. Soc. Jpn.*, 1999, **107**, 339–342.
8. Akimune, Y., Munakata, F., Matsuo, K., Okamoto, Y., Hirosaki, N. and Sato, C., Effect of grain size and grain structure on the thermal conductivity of β-Si_3N_4. *J. Ceram. Soc. Jpn.*, 1999, **107**, 1180–1182.
9. Watari, K., Hirao, K., Toriyama, M. and Kanzaki, S., Effect of grain size on the thermal conductivity of Si_3N_4. *J. Am. Ceram. Soc.*, 1999, **82**, 777–779.
10. Kitayama, M., Hirao, K., Toriyama, M. and Kanzaki, S., Thermal conductivity of β-Si_3N_4: I, Effects of various microstructural factors. *J. Am. Ceram. Soc.*, 1999, **82**, 3105–3112.
11. Kitayama, M., Hirao, K., Tsuge, A., Toriyama, M. and Kanzaki, S., Oxygen content in β-Si_3N_4 crystal lattice. *J. Am. Ceram. Soc.*, 1999, **82**, 3263–3265.
12. Kitayama, M., Hirao, K., Tsuge, A., Watari, K., Toriyama, M. and Kanzaki, S., Thermal conductivity of β-Si_3N_4 :II, Effects of lattice oxygen. *J. Am. Ceram. Soc.*, 2000, **83**, 192–198.
13. Li, B., Pottier, L., Roger, J. P., Fournier, D., Watari, K. and Hirao, K., Measuring the anisotropic diffusivity of silicon nitride grains by thermoreflectance microscopy. *J. Eur. Ceram. Soc.*, 1999, **19**, 1631–1639.
14. Xu, H. H. K., Wei, L., Padture, N. P., Lawn, B. R. and Yeckley, R. L., Effect of microstructural coarsening on Hertzian contact damage in silicon nitride. *J. Mater. Sci.*, 1995, **30**, 868–878.
15. Fabbri, L., Fournier, D., Pottier, L. and Esposito, L., Analysis of local heat transfer properties of tape-cast AlN ceramics using

photothermal reflectance microscopy. *J. Mater. Sci.*, 1996, **31**, 5429–5436.
16. Wei, L. and White, G. S., Thermal diffusivity maps: Case studies in ceramics. *J. Mater. Res.*, 1997, **12**, 2381–2387.
17. Williams, C. C. and Wickramasinghe, K., Scanning thermal profiler. *Appl. Phys. Lett.*, 1986, **49**, 1587–1589.
18. Nonnenmacher, M. and Wickramasinghe, K., Scanning probe microscopy of thermal conductivity and subsurface properties. *Appl. Phys. Lett.*, 1992, **61**, 168–170.
19. Majumdar, A., Carrejo, J. P. and Lai, J., Thermal imaging using the atomic microscope. *Appl. Phys. Lett.*, 1993, **62**, 2501–2503.
20. Maywald, M., Pylkki, R. J. and Balk, L. J., Imaging of local thermal and electrical conductivity with scanning force microscopy. *Scanning Microscopy*, 1994, **8**, 181–188.
21. Lever, T. J. and Price, D. M., Using microthermal analysis to characterize the nanoworld. *Am. Lab.*, 1998, **30**, 15–30.
22. Pollock, H. M. and Hammiche, A., Micro-thermal analysis: Techniques and applications. *J. Phys. D: Appl. Phys.*, 2001, **34**, R23–R53.
23. Ye, J., Kojima, N., Furuya, K., Munakata, F. and Okada, A., Microthermal analysis for determining thermal conductance distribution in advanced silicon nitride. *J. Thermal. Anal. Cal.*, 2002, **69**, 1031–1036.
24. Ye, J. and Okada, A., Micro-thermal analysis of head conduction in silicon nitrides. *J. Am. Ceram. Soc.* (in press).
25. Bando, Y., Mitomo, M. and Kurashima, K., An inhomogeneous grain boundary composition in silicon nitride ceramics as revealed by 300 kW field emission analytical electron microscopy. *J. Materials Synthesis and Processing*, 1998, **6**, 359–365.
26. Ruiz, F., Sun, W. D., Pollak, F. H. and Venkatraman, C., Determination of the thermal conductivity of diamond-like nanocomposite films using a scanning thermal microscope. *Appl. Phy. Lett.*, 1998, **73**, 1802–1804.
27. Asnin, V. M., Pollak, F. H., Ramer, J., Schurman, M. and Ferguson, I. T., High spatial resolution thermal conductivity of lateral epitaxial overgrown GaN/sapphire 0001 using a scanning thermal microscope. *Appl. Phy. Lett.*, 1999, **75**, 1240–1242.